CRYSTAL GROWTH & DESIGN

Article

pubs.acs.org/crystal

Rate of Lyotropic Nematic Phase Formation: Derivation and Application of Time−Concentration−Temperature−Transformation Diagrams

Jason Komadina,[†,‡] Stephen W. Watt,[§,‡] Iain J. McEwen,[⊥,∥] and Christopher Viney*[,†]

[†]School of Engineering, University of California at Merced, Merced, California 95343, United States

[§]Solid Form Solutions Limited, Milton Bridge, Near Penicuik, Scotland EH26 0BE, United Kingdom

[⊥]Department of Chemistry, Heriot-Watt University, Edinburgh EH14 4AS, United Kingdom

Supporting Information

ABSTRACT: The effect of both temperature and composition on the rate of transformation of a nematic phase from an isotropic solution is examined from a theoretical standpoint. The kinetics of the transformation are presented as a time−concentration−temperature−transformation (TCTT) diagram, analogous to the time−temperature−transformation (TTT) diagrams commonly used in metallurgical process design. The transformation is regarded as a nucleated process in which the transformation rate is proportional to the number of stable nuclei, and this in turn depends on a balance between the energy gained by nematic ordering and the energy expended in forming the nematic−isotropic interface. The nematic ordering term is estimated as a function of both concentration and temperature via two different approaches: (i) the lattice theory as described by Flory and Warner and (ii) the Maier−Saupe theory of nematic ordering. Although there are differences in detail, both approaches yield the same qualitative result. The present work provides the details necessary for developing a specific example application of our recently reported generalized system-independent model of nucleation and growth. The TCTT diagram is in essence a phase diagram augmented by kinetic information for nematic ordering, and thus is expected to be a powerful graphical tool in liquid crystal process engineering and other applications.

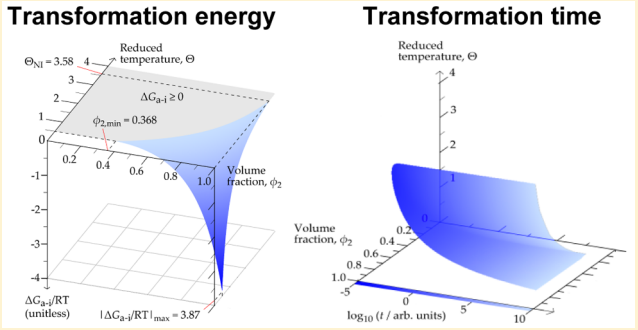

INTRODUCTION

Nucleation and growth theory has been applied to a broad range of phase transformation phenomena that exhibit a competition between favorable transformation energy and unfavorable surface energy. Indeed, classical nucleation theory, originally derived for condensation of vapor to liquid,[1,2] is now commonly taught in introductory materials science courses in terms of the heat treatment of steels.[3−8] Classical nucleation and growth theory applies equally well to crystallization (of ice,[9] proteins from solution,[6,10−13] and colloids[13,14]), liquid crystalline phase formation,[15−17] and even fields outside of the physical sciences, such as epidemiology.[18] In the case of metallurgical,[3,19,20] ceramic,[21] and mineral[22] phase transformations, the kinetic behavior that results from nucleation and growth is commonly represented on a time−temperature−transformation (TTT) diagram. Such diagrams display contours, often "C" shaped, of constant transformed fraction plotted on the temperature−time plane and are valuable graphical tools for process engineering.

An analogous example is found in the transformation from an isotropic solution to a lyotropic nematic liquid crystalline phase, discussed in McEwen[23] and in the present work. The nematic phase becomes thermodynamically favored at a critical mesogen concentration, with the overall free energy becoming more negative as the concentration of the mesogen is further increased. Given this increasing thermodynamic "drive", the number of nuclei and the rate of nematic phase growth should be an increasing function of concentration. However, since increased concentration also reduces mass transport rates, the overall rate of nucleation and growth necessarily exhibits a maximum at some optimum concentration. Such behavior has been observed experimentally[24,25] during the formation of liquid crystalline phases from three biological polymers in solution—silk fibroin (a protein), levan (a polysaccharide), and mucin (a glycoprotein). Assuming a fixed temperature, this situation can be conveniently visualized in terms of a time−concentration−transformation (TCT) "C curve", such as shown in McEwen et al.[23]

A complete picture of the rate at which nematic (or other) structures nucleate and grow from solution should logically include any possible effect of temperature. Although wide temperature variations are unlikely in the context of phase

Received: September 29, 2014
Revised: March 18, 2015
Published: March 31, 2015

DOI: 10.1021/cg501459m
Cryst. Growth Des. 2015, 15, 2620−2631

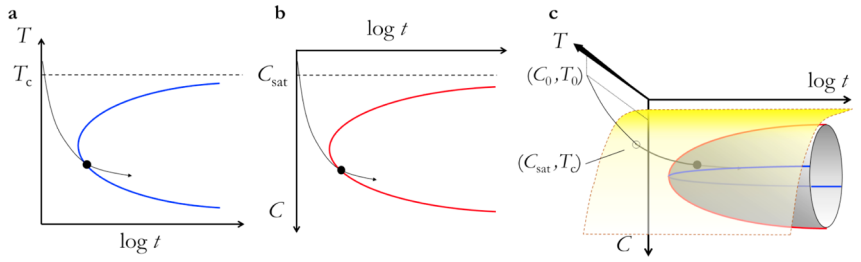

Figure 1. Schematic illustrations of (a) a time−temperature−transformation (TTT) diagram for a system with fixed composition and $T < T_c$, (b) a time−concentration−transformation (TCT) diagram at constant temperature and $C > C_{sat}$, and (c) a time−concentration−temperature−transformation (TCTT) diagram, allowing for simultaneous change in T and C. TTT and TCT diagrams in a and b are effectively cross sections of the TCTT diagram in c. In each illustration, a process pathway (black arrow; one of many possibilities) shows a change in the relevant system variable(s) over time; a lag between phase transformation becoming favorable (crossing the critical value in temperature and/or concentration) and 1% transformation time (black dot) is apparent.

transformations exploited in Nature, where the range of any particular habitat is limited, temperature is a potential—and perhaps useful—variable in the production of synthetic liquid crystalline material from isotropic solution. Recently, we presented[26] a generalized model that allows nucleation and growth to be driven by simultaneous changes in multiple system variables. The general model is based on classical considerations of the overall free energy of a growing nucleus in terms of a balance between the "benefit" of free energy decrease due to phase transformation and the free energy "cost" of maintaining an interface between the initial and the product phases. We showed how transformation diagrams analogous to the TTT diagram are expected to arise in a wide range of phenomena in materials science and other contexts. We then showed how such transformation diagrams can be a useful tool for communicating kinetic data and designing process pathways. In particular, we described the rationale for, and schematically illustrated, time−concentration−temperature−transformation (TCTT) diagrams applicable to the precipitation of solid from a liquid solution. The TCTT diagram concept expands on the TCT diagram by considering phase transformation driven by simultaneous change in concentration and temperature.

Figure 1 schematically illustrates the TTT, TCT, and TCTT concepts. In the TTT diagram represented in Figure 1a, the blue C curve represents the time required at a given temperature, T, less than some critical temperature, T_c, to transform a particular fraction of material (e.g., 1%) in a system with fixed concentration. Figure 1b shows a schematic TCT diagram at constant temperature, where the red C curve represents the 1% transformation time for a given concentration, C, greater than the saturation concentration, C_{sat}. Finally, the two concepts are combined in a TCTT diagram in Figure 1c, where the saturation condition (C_{sat}, T_c) is represented by a curved surface (yellow) parallel to log t, qualitatively acknowledging that C_{sat} will in general depend on T. The gray cup-shaped surface represents the 1% transformation time for the range of C and T over which transformation is favorable. The blue and red C curves from Figure 1a and 1b are superimposed on the surface in Figure 1c to emphasize that TTT and TCT diagrams are essentially cross sections of the TCTT diagram.

We argued[26] that TCTT (and similar) diagrams would be useful in designing processes that favor controlled formation of a specific phase during, for example, drug development and manufacturing. We noted that effective use of the general model requires sufficient knowledge of the system in question in order to reasonably estimate values of the phase transformation energy, surface energy, and important system parameters.

In the present paper, we examine the theory of liquid crystal formation to take account of simultaneous changes in concentration and temperature and to gain some insight into the likely consequence of such changes. In particular, the free energy of transformation and the corresponding critical nucleation energy are modeled, and the corresponding rate of nucleation and TCTT behavior are calculated. We use several simplifying assumptions regarding the nature of the mesogen−solvent system, our principal aim being to showcase the TCTT diagram for this type of application, leaving more accurate representation of aspects such as the detailed behavior of specific mesogens for future publication.

In some respects we were prompted to develop the theoretical rationale[23,26] of TCT and TCTT behavior outlined above by the widespread incidence of liquid crystallinity in Nature and by the recognition[27] that various structural natural materials show an organization which is reminiscent of a precursor liquid crystalline phase. The actual rate at which a transformation to liquid crystalline order occurs must itself be of some consequence when assembly has to occur under time-sensitive conditions—as, for example, is the case during the production of silk fibers by spiders. Natural silk is spun in a process which requires rapid water loss from the nascent fiber by reabsorption within the spinneret and which could be usefully described in the language of TCT/TCTT diagrams. More broadly—though not attempted in the present paper—we envisage that our generalized approach to modeling nucleation and growth for a phase transition driven by simultaneous changes in multiple system variables[26] can incorporate an important rheological element into our understanding of liquid crystal polymers,[28] ultrahigh-modulus polymers,[29,30] or the role played by liquid crystallinity in the spinning of natural silk.[31]

THEORY AND MODELING

Our previous treatment of nematic ordering[23] adapted the classical approach[4] of metallurgy to describing nucleation and growth processes but considered only the effect of composition on the free energy of lyotropic liquid crystal phase formation, $\Delta G_{a\text{-}i}$. In the present paper we apply and compare two approaches which allow us to also incorporate the effect of temperature into $\Delta G_{a\text{-}i}$, namely, an extended Flory lattice model[32−35] and the Maier−Saupe (MS) theory[36,37] for liquid crystal formation. The latter is a mean field theory in which free

DOI: 10.1021/cg501459m
Cryst. Growth Des. 2015, 15, 2620−2631

energy depends on the orientational order (an entropy contribution) and a temperature-dependent interaction parameter. However, it takes no account of the specific shape of the molecules involved and so does not incorporate the axial ratio of the mesogens into its predictions; instead, orientational order is quantified in terms of how closely the dipoles induced on the mesogens by anisotropic dispersion forces are aligned relative to the local average direction of such dipoles. The Flory approach, in contrast, evaluates the appropriate combinatorial partition function specifically in terms of the axial ratio, which itself is defined in terms of contiguous lattice sites. The lattice approach emphasizes the major contribution of steric repulsions, and although in its simplest form the theory is athermal, it was later extended[33−35] to account for "soft" orientation-dependent molecular interactions as now outlined. This extended Flory−Warner (FW) approach is used in the present work.

Flory−Warner Approach. The thermodynamic drive for the formation of a lyotropic liquid crystalline phase can be expressed as the difference between the free energy of mixing for solvent and mesogen in the isotropic state, ΔG_i, and the free energy of mixing for solvent and mesogen in the anisotropic state, ΔG_a. The free energy difference between an anisotropic mixture and the corresponding isotropic mixture, $\Delta G_{a\text{-}i} = \Delta G_a - \Delta G_i$, can be stated conventionally in terms of mole fraction composition, X_i, by

$$\Delta G_{a-i} = [X_1(\mu_1 - \mu_1^\circ) + X_2(\mu_2 - \mu_2^\circ)]_a - [X_1(\mu_1 - \mu_1^\circ) + X_2(\mu_2 - \mu_2^\circ)]_i \quad (1)$$

where component 1 is the solvent and component 2 is the mesogen, μ_j is the chemical potential (partial molar free energy) of component j in solution, and μ_j° is the chemical potential of component j in its standard state.

The original lattice theory considered such mixtures to be made up of "hard rods", devoid of any interactions other than an infinitely large contact repulsion, and predicts that the formation of a nematic phase depends solely on the rod concentration and the rod axial ratio. The problem of ordering rods to allow for the effect of temperature was addressed by Flory and Ronca,[33] still within the lattice framework, but by additionally incorporating soft anisotropic dispersion forces as a perturbation. This approach was refined by Flory and Warner, and here we employ the expressions for chemical potentials as given in their paper[34] to introduce a temperature dependence into eq 1. The excess chemical potentials for the solvent (component 1) in the anisotropic and isotropic phases are, respectively

$$\frac{(\mu_1 - \mu_1^\circ)_a}{RT} = \ln(1 - \phi_2) + a + \frac{\phi_2}{x}(\hat{y} - 1) + \frac{\phi_2^2 s^2}{2\Theta} \quad (2)$$

$$\frac{(\mu_1 - \mu_1^\circ)_i}{RT} = \ln(1 - \phi_2) + \frac{\phi_2}{x}(x - 1) \quad (3)$$

For the mesogen (component 2)

$$\frac{(\mu_2 - \mu_2^\circ)_a}{RT} = \ln\left(\frac{\phi_2}{x f_1}\right) + \phi_2(\hat{y} - 1) - \frac{x\phi_2 s}{\Theta}\left(1 - \frac{\phi_2 s}{2}\right) \quad (4)$$

$$\frac{(\mu_2 - \mu_2^\circ)_i}{RT} = \ln\left(\frac{\phi_2}{x}\right) + \phi_2(x - 1) \quad (5)$$

where ϕ_2 is the volume fraction of rods, x is the axial ratio of a rod, and the variable Θ is a reduced temperature, $\Theta = T/T^*$, where $k_B T^*$ defines the energy of interaction between rods. The parameter a is given by

$$a = -\ln\left[1 - \phi_2\left(\frac{1 - \hat{y}}{x}\right)\right] \quad (6)$$

where the disorder index, $\hat{y}$, is the projection of a rod onto the plane perpendicular to the preferred direction and s is an order parameter. These are defined by

$$\hat{y} = \frac{4x}{\pi}\left(\frac{f_2}{f_1}\right) \quad (7)$$

$$s = \frac{1}{2}(3\langle\cos^2\theta\rangle - 1) = 1 - \frac{3f_3}{2f_1} \quad (8)$$

where $\langle\cos^2\theta\rangle$ is the ensemble average of $\cos^2\theta$, with θ being the angle between the mesogen and the direction of preferred orientation. The quantities f_j above are the jth moments of the distribution of mesogen orientation

$$f_j = \int_0^{\pi/2} (\sin^j\theta)\exp\left[-x\left(\frac{4a}{\pi} + \frac{3\phi_2 s}{2\Theta}\sin\theta\right)\sin\theta\right]d\theta \quad (9)$$

where the integration is taken from $\theta = 0$ (rods parallel to preferred direction) to $\theta = \pi/2$ (rods normal to preferred direction).

To determine the free energy of transformation from eqs 1−5, eqs 6−9 must first be solved iteratively, as described by Yoon and co-workers.[38] Initial guesses of $a = 1$ and $s = 0.25$ (chosen based on the allowed range of each) were inserted into eq 9, which was numerically integrated to yield values of f_1, f_2, and f_3, from which refined values of a and s were then calculated. This iteration was performed until the difference in $|a|$ and $|s|$ per iteration was less than 10^{-6}. The calculation converged within 100 iterations for >99% of the range of Θ and ϕ_2; time-out errors occurred only for points on or very close to the nematic−isotropic transition.

The value of the axial ratio was set to $x = 5$, less than the critical value of 6.417 needed to ensure that some contribution from soft interactions is required to yield liquid crystal formation regardless of rod concentration,[33,35] and therefore provides a defensible basis for comparison with the predictions of the MS approach. The range for reduced temperature was arbitrarily set to $0.5 \le \Theta \le 4$.

A value for the equation-of-state interaction term T^* is needed to relate reduced temperature to actual temperature. Flory and Irvine[39] applied two approaches in evaluating this parameter for a series of low molar mass rigid polyphenyl mesogens, both effectively using equation-of-state data under equilibrium conditions, with $T = T_{NI}$, the clearing temperature. Experimental data for model systems are sparse, and other researchers,[38] working with a semiflexible liquid crystalline polymer, simply estimated T^* by matching plots of experimental and theoretical values of T_{NI}, and alternatively by matching the theoretical and experimental boundaries on phase diagrams. The differences in T^* values obtained by these

DOI: 10.1021/cg501459m
Cryst. Growth Des. 2015, 15, 2620−2631

two fitting methods was considerable, implying that T^* may be a rather imprecise parameter in complex molecules where the mesogenic unit itself is difficult to define. Accepting this, we proceed on the basis that a reasonable matching of our FW and MS calculation results is obtained by setting T^* to 167.6 K. Further justification for this choice is provided in the Results and Discussion.

Maier−Saupe Approach. Maier and Saupe[36,37] approached the problem of nematic−isotropic equilibria by considering that the dispersion forces between mesogens provide the only aligning influence, with shape anisotropy and lattice effects not being considered important. The free energy of anisotropic ordering, $g^n = \Delta G_{a\text{-}i}/RT$, is obtained[40,41] from the more general expression derived by Brochard and coworkers[42] as

$$g^n = \phi_2 \int_\Omega f(\theta)\ln[4\pi f(\theta)]\,d\Omega - \frac{1}{2}\nu\phi_2^2 s^2 \tag{10}$$

where the integral is evaluated over all solute orientations, the differential solid angle is given by $d\Omega = \sin\theta\ d\theta\ d\psi$ in polar coordinate representation, s is defined in eq 8, and ν is the temperature-dependent Maier−Saupe interaction parameter which is related to the clearing temperature T_{NI} by

$$\nu = \frac{4.54T_{NI}}{T} \tag{11}$$

The normalized orientation distribution function, $f(\theta)$, is connected to the partition function, Z, and a mean field parameter, m, by

$$f(\theta) = \frac{1}{4\pi Z}\exp\left(\frac{-u(\theta)}{k_B T}\right) \tag{12}$$

$$\frac{u(\theta)}{k_B T} = -\frac{1}{2}m(3\cos^2\theta - 1) \tag{13}$$

The first (integral) term in eq 10 is the entropic orientational order term, and the second term represents the energy of mesogen−mesogen interaction; the MS calculations in this work neglect mesogen−solvent interaction energy. A methodology for solving eqs 10−13 is provided by de Gennes;[43] we adapted this approach as used by Chiu.[41] The mathematical methods are presented in detail in sections S1−S3 in the Supporting Information. The selection of clearing temperature can be arbitrary for the purpose of illustration of predicted system behavior; the value of 600 K used here can be justified practically because it is comparable to the clearing temperature of model (tolane-based) compounds[44,45] for which $x = 5$, as used above in the FW approach to calculating free energy. The lower limit for T in the MS calculation was set arbitrarily to 100 K.

Nucleation Rate and Phase Growth. As before,[23] we envisage small regions of order, arising from density fluctuations, acting as the nuclei for phase growth. We briefly described such a scenario in the context of the general model[26] as well. Applying the classical view of nucleation,[4] these small nuclei of ordered solution respond to two opposing effects: a favorable contribution from $\Delta G_{a\text{-}i}$, proportional to the volume of the nucleus, and an unfavorable surface free energy contribution proportional to its surface area. The relationships in this section are commonly used to describe classical nucleation, and derivations may be found in greater detail in our previous work[23,26] and indeed in introductory materials science textbooks[7,8] in the context of metallurgical phase transformation. The energy of homogeneous nucleation, ΔG_n, for a spherical nucleus of radius r is

$$\Delta G_n = \frac{4}{3}\pi r^3 \Delta G_{a-i} + 4\pi r^2 \gamma \tag{14}$$

We made the spherical nucleus assumption to simplify some of the theoretical treatment and illustrate TCTT behavior for the present application without too much distraction from the central ideas. Spherical nuclei of a critical size that promotes further growth have a critical free energy of nucleation

$$\Delta G_c = \frac{16\pi\gamma^3}{3(\Delta G_{a-i})^2} \tag{15}$$

where $\Delta G_{a\text{-}i}$ is scaled per unit volume and in the present work is calculated by either the FW or MS method. The surface energy, γ, is scaled per unit area of the interface between the ordered nucleus and the isotropic solution, which results in ΔG_c with units of energy. Real nematic phases are unlikely to have uniform surface energy, due to the preferred orientation of mesogen, and a more accurate representation of γ should include considerations for nonuniformity. Along these same lines, the growth rate of nuclei is unlikely to be isotropic or constant, since an approaching mesogen will necessarily interact differently with the nuclei depending on its orientation relative to the director. Similarly, local gradients in composition, temperature, and nucleus shape are likely to have significant impacts on the nucleation and growth behavior but are left for future refinement of the model for real systems.

The equilibrium number of critical nuclei n_c is related to the total number of *possible* (stable and unstable) nuclei, N_0, and the critical nucleation energy

$$\frac{n_c}{N_0} = \exp\left(\frac{-\Delta G_c}{k_B T}\right) \tag{16}$$

The rate of nucleation, i.e., the rate of formation of stable nuclei, is proportional to n_c. Progression from a critical nucleus to a stable nucleus in our system requires the addition of one more mesogen, which is assumed to be controlled by the rate at which mesogens can diffuse to the nuclei from the isotropic solution. Thus, the rate of nucleation is also proportional to the rate of mass transport to the nucleation site, which may be taken in turn as proportional to diffusivity, D. It is reasonable to assume an exponential concentration dependence[46] for diffusion

$$D = D'\exp(-\beta\phi_2) \tag{17}$$

where β represents a decay constant for concentration dependence of diffusion. Temperature dependence is then sensibly introduced by

$$D' = D_0 \exp\left(\frac{-Q_d}{k_B T}\right) \tag{18}$$

where Q_d is an activation energy term. We may combine eqs 15−18 to obtain an expression for the overall nucleation rate, $I = \partial N/\partial t$, where N is the number of stable nuclei, in terms of both the solution concentration and the temperature

$$I \propto D_0 N_0 \exp[(-\Delta G_c/k_B T) - \beta\phi_2 - (Q_d/k_B T)] \tag{19}$$

DOI: 10.1021/cg501459m
Cryst. Growth Des. 2015, 15, 2620−2631

with $\Delta G_c = \Delta G_c(\phi_2, T)$ obtained by inserting either of the treatments outlined in the previous sections for $\Delta G_{a\text{-}i}$ into eq 15.

The result in expression 19 is consistent with the general model that we recently reported, when the latter is applied to the specific case of nucleation dependent on two system variables in a diffusion-limited system. The generalized form of the nucleation rate, as presented in our previous report,[26] is reproduced below for reference. Note that in the context of expression 20, m represents the number of system variables being considered.

$$\frac{\partial N}{\partial t} \propto \left[N_0 \exp\left(\frac{-\Delta G_c(\xi_1, \ldots \xi_m)}{\kappa}\right)\right]\left[D_0 \exp\left(-\sum_i^m \beta_i \xi_i^{\alpha_i}\right)\right] \tag{20}$$

The consistency between the general expression 20 and the two-variable expression 19 of present interest is clear when the following equivalences are noted: $\xi_1 = \phi_2$, $\xi_2 = T$, $\alpha_1 = 1$, $\alpha_2 = -1$, $\beta_1 = \beta$ (unitless), $\beta_2 = Q_d/k_B$ (units of temperature, K), and $\kappa = k_B T$. We previously used molar concentration, C, to assist in illustrating the generality of the model and how one might treat various model parameters in the context of a concentration-driven nucleation process. Here, the use of ϕ_2 in place of C ensures consistency with the FW and MS approaches for estimating the free energy of transformation.

The proportionality in eq 19 has been addressed previously by several authors and typically[14,47−49] includes a factor originally derived from statistical thermodynamic principles by Zeldovich.[50] The fact that a particular nucleus has reached critical size does not *require* the nucleus to continue growing; it merely stipulates that further growth is energetically favored. The Zeldovich factor, z, represents the probability of a critical nucleus increasing in size and may be expressed as

$$z = \sqrt{\frac{-1}{2\pi k_B T}\left(\frac{\partial^2 \Delta G_n}{\partial n^2}\bigg|_{n=n^*}\right)} = \frac{V_{mol}[\Delta G_{a-i}(\phi_2, T)]^2}{8\pi\sqrt{k_B T \gamma^3}} \tag{21}$$

where n represents the number of basic units (atoms, molecules, unit cells) in the nucleus, n^* is the number of basic units in a critical nucleus, and V_{mol} is the molar volume of the nucleating phase such that $(4/3)\pi r^3 = nV_{mol}$. In the present work, we assumed that the surface energy is approximately constant with volume fraction, ϕ_2, and temperature, T. In our previous treatments,[23,26] we were satisfied to show the proportionality expression in eq 19 as a first-order model of phase transformation and therefore did not include consideration of the prefactor. Our reasoning was that, although the prefactor represented by eq 21 clearly exhibits dependence on $\Delta G_{a\text{-}i}(\phi_2, T)$, the exponential terms in expression 19 dominate the overall nucleation rate. In the present work, where we are concerned with modeling phase transformation in a specific type of system, over a wide range of concentration and temperature, we included the Zeldovich factor; its quantitative contribution to the predictions is addressed in the Results and Discussion. Thus, we rewrite expression 19 to include z

$$I \propto zD_0N_0 \exp[(-\Delta G_c/k_B T) - \beta\phi_2 - (Q_d/k_B T)] \tag{22}$$

We note that the above expression remains a proportionality, since the mass transport term has not been fully accounted for by diffusivity but requires consideration of the flux near the surface of the critical nuclei as well.

TCTT Diagrams. We discussed the utility of TCT and TCTT diagrams at length in our previous work[23] and in the context of the general model for nucleation and growth,[26] respectively. In this section, we describe our method for calculating TCTT diagrams for lyotropic liquid crystal phase formation. The fraction of transformed material, Y, at a particular time, t, may be expressed using the well-known Avrami equation[51,52]

$$Y = 1 - \exp(-Kt^p) \tag{23}$$

where K is a function of nucleation rate, growth rate, and nucleus geometry; p is the "Avrami factor", which depends on the nature of the nucleation (instantaneous or sporadic) and the dimensionality (sphere, disc, etc.). To determine the time required to achieve a particular value of Y, we may rearrange eq 23 to write

$$t^p = \frac{-\ln(1 - Y)}{K} \tag{24}$$

Small changes in supercooling or supersaturation often result in order-of-magnitude changes in the kinetics of phase transformation. Thus, it is more common to consider time on a logarithmic scale

$$\log_{10} t = \frac{1}{p}\log_{10}\left(\frac{-\ln(1 - Y)}{K}\right) \tag{25}$$

We now assume that the homogeneous formation of the spherical nuclei of the anisotropic phase occurs sporadically. We also assume that the nucleation rate, $I = \partial N/\partial t$, and growth rate, $\partial r/\partial t$, are both independent of time. These assumptions simplify our calculations but are flawed, since they require also that $\partial\phi_2/\partial t = 0$ (isotropic phase behaves as a reservoir) and $\partial T/\partial t = 0$ (isothermal phase transformation). The assumptions above allow us to use $K = kI(\partial r/\partial t)^3$ and $p = 4$, where the shape factor, k, is equal to $\pi/3$ for spherical nuclei[51,52]

$$\log_{10} t = \frac{1}{p}\log_{10}\left(\frac{-\ln(1 - Y)}{kI\left(\frac{\partial r}{\partial t}\right)^3}\right) \tag{26}$$

In deriving expression 19, we assumed a diffusion-limited system. Thus, we consider that the growth rate is proportional to the mass transport rate. We may now write an explicit expression for $\log_{10} t$ using the system parameters and critical nucleus energy derived by the FW and MS calculations

$$\log_{10} t = A + \frac{1}{4}\left[\log_{10}(-\ln[1 - Y]) - \log_{10} kz + \frac{1}{\ln 10}\left(\frac{\Delta G_c}{k_B T} + 4\left[\beta\phi_2 + \frac{Q_d}{k_B T}\right]\right)\right] \tag{27}$$

where A encapsulates the various constants of proportionality. The resulting TCTT diagrams show surfaces of constant Y in temperature−concentration−time space. The value of A can be estimated by comparing results from experiment and simulation. We note that according to eq 27, changes in A or Y should not affect the *shape* of the TCTT surfaces in our present treatment but should merely shift them along the time axis. However, the shape of the TCTT surfaces will be directly influenced by the nucleus geometry (via the relationship between ΔG_c and $\Delta G_{a\text{-}i}$), the assumptions of isotropic growth,

DOI: 10.1021/cg501459m
Cryst. Growth Des. 2015, 15, 2620−2631

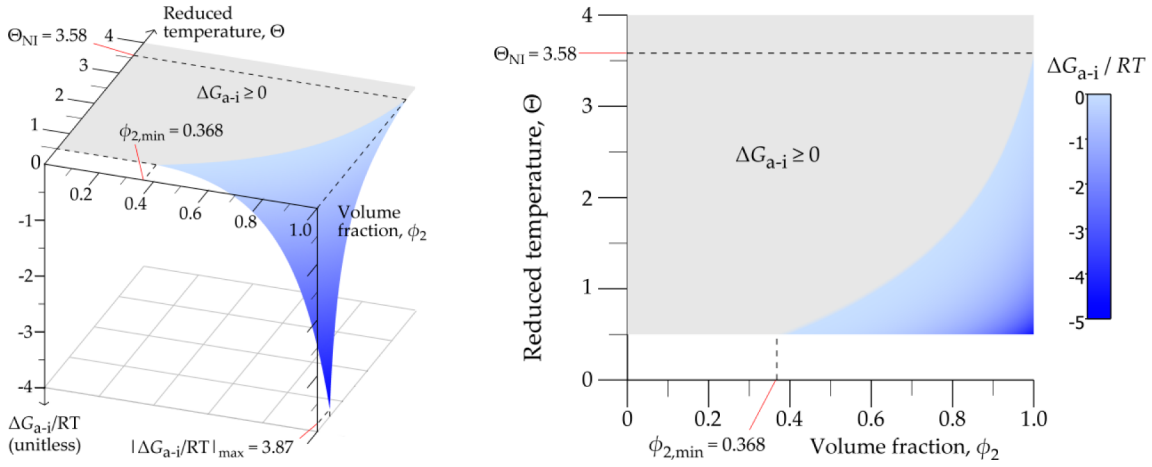

Figure 2. Free energy of phase transformation, $\Delta G_{a\text{-}i}$, as a function of volume fraction, ϕ_2, and reduced temperature, Θ, calculated from Flory–Warner (FW) theory for an axial ratio of $x = 5$. The minimum volume fraction for phase transformation and the reduced clearing temperature are indicated. The right-hand plot shows a "top-down" view along the free energy axis.

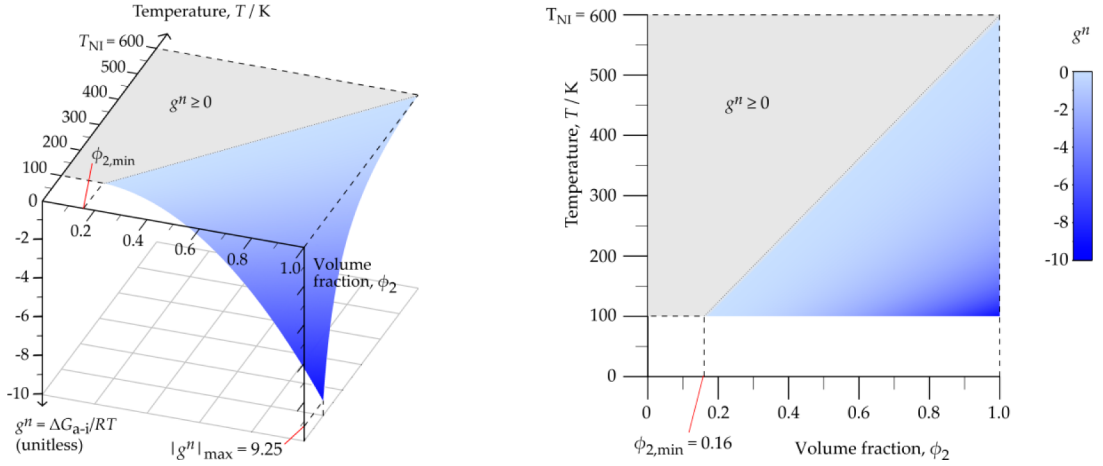

Figure 3. Free energy of transformation, $g^n = \Delta G_{a\text{-}i}/RT$, as a function of volume fraction, ϕ_2, and temperature, T, calculated from Maier–Saupe (MS) theory for a clearing temperature of $T_{NI} = 600$ K. The right-hand plot shows a "top-down" view along the free energy axis.

and the assumptions that T and ϕ are constant in time. These considerations have been ignored in the present work for the sake of simplicity of argument in demonstrating the model and TCTT surfaces as a framework for phase transformation process design.

All of the calculations described above were performed using custom scripts in FreeMAT. The plots were generated using QtiPlot.

RESULTS AND DISCUSSION

Free Energy of Phase Transformation. The results of the FW calculations for energy of transformation are shown in Figure 2 for $x = 5$ over the arbitrary reduced temperature range $0.5 \leq \Theta \leq 4$. At the lowest reduced temperature shown, a stable nematic phase appears near $\phi_2 = 0.37$. The range of volume fraction over which $\Delta G_{a\text{-}i} < 0$ then contracts with increasing reduced temperature, with a reduced clearing temperature located near $\Theta = 3.58$. The FW theory thus successfully predicts a *reduced* thermotropic clearing point, at least for small values of the axial ratio, but still requires an independent estimate of the interaction term T^* in order to convert to actual clearing temperatures. As the axial ratio, x, increases, Θ_{NI} rapidly approaches unrealistically large values[33,34] as illustrated by Figure S1, Supporting Information.

Since the values of $\Delta G_{a\text{-}i}/RT$ calculated by the FW method are only dependent on the reduced temperature, the choice of T^* effectively acts to scale the results to a set of absolute temperature values, needed for calculating the rate of nucleation. In the present calculations, we set $T^* = 167.6$ K to match the reduced clearing temperature of $\Theta = 3.58$ with $T_{NI} = 600$ K, used in the MS calculations. By defining T^* in this way, the results from the FW calculation are based on the same temperature scale as the MS calculation, and both calculations effectively use the same clearing temperature.

The values of $\Delta G_{a\text{-}i}$ calculated by the MS procedure are shown in Figure 3. At the lowest temperature in our calculations, 100 K, nucleation is unfavorable for volume fraction less than $\phi_2 = 0.16$. The general shape of the negative free energy region is comparable to that calculated from FW theory; however, the curvature in Figure 2 is more marked, and nonlinear temperature dependence for the minimum concentration for nematic ordering is predicted by FW theory, as opposed to the linear dependence obtained from MS theory as in Figure 3.

DOI: 10.1021/cg501459m
Cryst. Growth Des. 2015, 15, 2620–2631

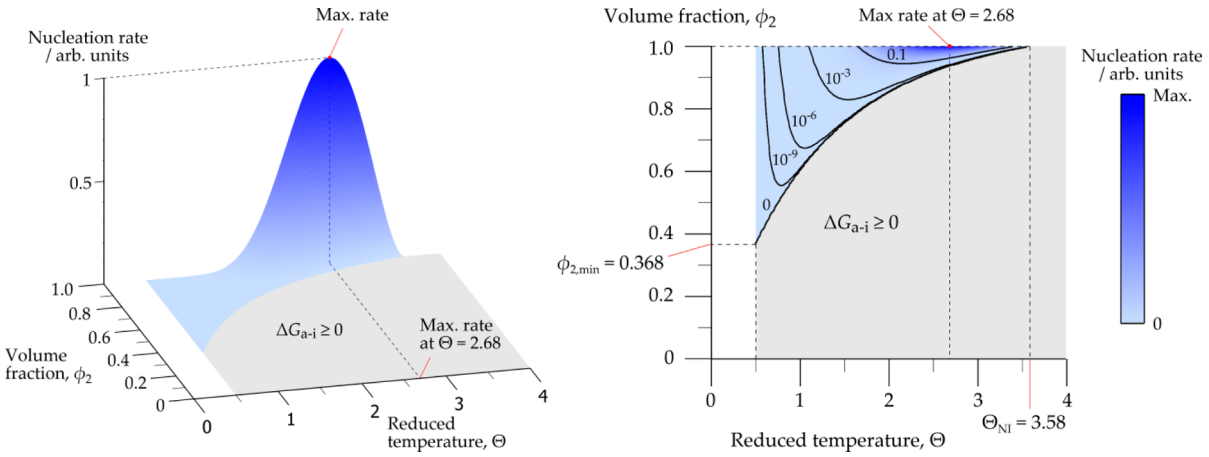

Figure 4. Relative rate of nucleation predicted from the FW free energy data of Figure 2, with $Q = 2000$ K, $\beta = 3$, and $T^* = 167.6$ K (selected to match Θ_{NI} with $T_{NI} = 600$ K in MS calculations). The maximum rate occurs at $\Theta = 2.68$, or $T \approx 449$ K. The right-hand plot is a top-down view along the rate axis. Black curves are contours of constant nucleation rate (labeled next to the contour) relative to the maximum rate calculated by the FW method. [Axis orientation changed from that in Figure 2 for clarity in displaying the nucleation rate data.]

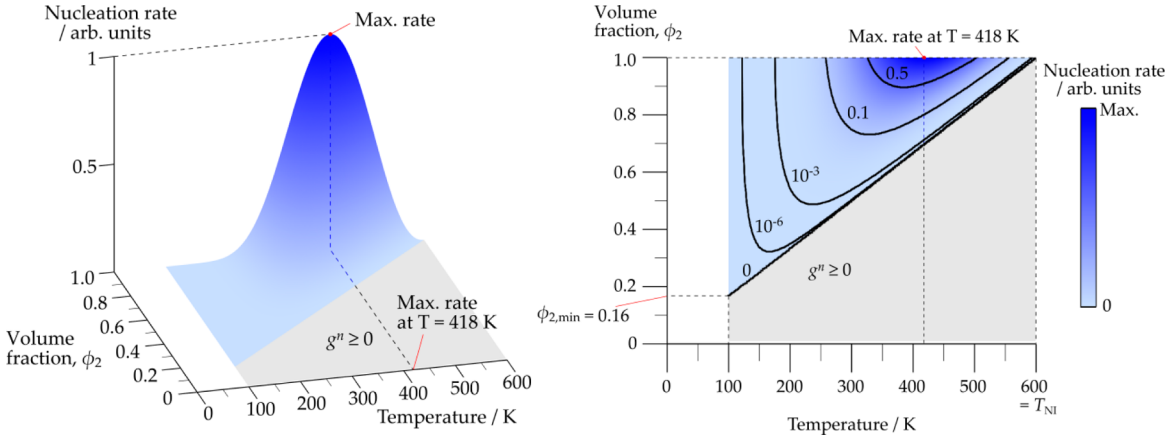

Figure 5. Relative rate of nucleation predicted from the MS free energy data of Figure 3, with $Q = 2000$ K, $\beta = 3$, and $T_{NI} = 600$ K. The maximum rate occurs at $T = 418$ K. The right-hand plot is a top-down view along the rate axis. Black curves are contours of constant nucleation rate (labeled next to the contour) relative to the maximum rate calculated by the MS method. [Axis orientation changed from that in Figure 3 for clarity in displaying the nucleation rate data.]

A strict comparison between the two approaches is difficult because the effect of axial ratio is not considered explicitly by the MS theory. However, since the consequence of increasing axial ratio, *mutatis mutandis*, is an increase in clearing temperature, the choice of T_{NI} in MS theory may be regarded as a default choice of axial ratio. Setting, for the FW case, $T^* = 167.6$ K with $x = 5$ effectively matches T_{NI} in the two approaches. The onset concentrations for nematic ordering at lower temperatures remain less well matched. This result is perhaps unsurprising, since the onset concentration is related explicitly to the axial ratio of the mesogen in the FW method, whereas in the MS description the onset concentration is a function of the undercooling $(T_{NI} - T)$. Since both the FW and the MS approaches yield similar but not identical predicted behavior, the results shown in Figures 2 and 3 are each applied to the prediction of nucleation rates.

Nucleation Rate. The exponential expression 19 is a first-order description of the relative rate of nematic phase growth in an isotropic solution when it is brought into a thermodynamically stable anisotropic region by changing the temperature and/or the concentration. Although the transport processes by which this occurs will depend on the mobility of both mesogen and solvent, they are described here by simple global terms $Q = Q_d/k_B$ and β. It is expected, however, that motion of the mesogen will dominate the ordering process, with the greatest concentration dependence occurring for polymeric solutes. To determine a reasonable upper bound for β, we fitted the diffusion data published by Russo and co-workers[53] for isotropic solutions of poly(γ-benzyl α,L-glutamate) (PBLG, 20×10^3 g mol^{-1} in pyridine) to an exponential to give $\beta \approx 9$. For shorter mesogens, diffusion will be less concentration dependent, with β tending to zero in systems where solvent and mesogen are of comparable mobility. We set $\beta = 3$ for the nucleation rate calculations in the present work.

A realistic limit to the value of the activation term Q can be estimated from literature data for low molar mass mesogens[54] of the N=N or N=C linked phenyl type, which indicate Q values to lie in the range 1800−4900 K. For a cyanobiphenyl-type mesogen, Vilfan and co-workers[55,56] find that $Q = 4050$ K describes their isotropic diffusion data. The data provided by Russo and co-workers[53] indicate that a Q value of ∼2300 K should characterize the zero concentration diffusion dependence of PBLG in isotropic solution. Since we were guided by that study in our choice of β, we set Q equal to 2000 K in an

DOI: 10.1021/cg501459m
Cryst. Growth Des. 2015, 15, 2620−2631

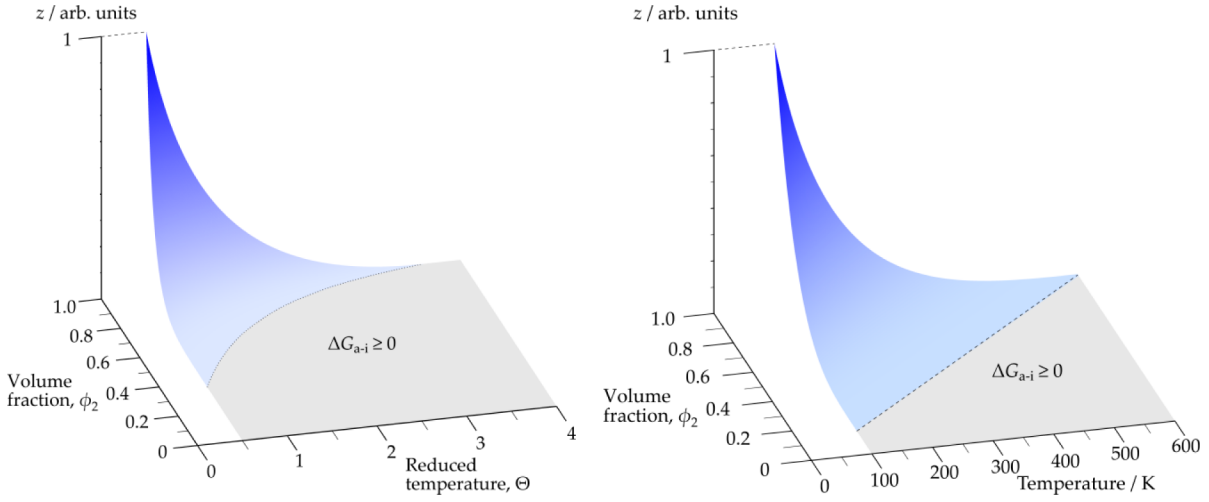

Figure 6. Zeldovich factor is plotted for the FW (left) and MS (right) calculations using T^* = 167.6 K and T_{NI} = 600 K, respectively. The trend of the Zeldovich factor toward zero near the isotropic−nematic transition is significant in that it severely limits the rate of transformation near this line.

attempt to achieve internal consistency for the calculations in the present work.

We adopted[23] a value of $\gamma = 2 \times 10^{-9}$ J cm^{-2}, on the basis of literature data.[57−60] The molar volume of the nucleating nematic phase, V_{mol}, is semiarbitrarily set equal to 100 cm^3 mol^{-1}, approximately 5 times that of water and therefore reasonably consistent with the selected axial ratio. Figures 4 and 5 show the relative rates of anisotropic phase nucleation, calculated from the free energy results by the FW and MS methods, respectively.

The nucleation rates shown in Figures 4 and 5 are normalized by the maximum value attained for each of the calculations. The expressions used to calculate rate are stated in the present work as proportionalities, and thus, any numerical result is inherently normalized by the constants of proportionality that are not explicitly addressed. Furthermore, the FW and MS methods are not directly comparable, so little value if any is added by giving the actual rate. The major difference in the outcome of the rate calculations is the slightly larger "footprint" within which finite transformation rates occur in the MS approach (Figure 5) compared to the FW approach (Figure 4), which follows simply from the larger $\Delta G_{a\text{-}i} < 0$ region in the energy calculations. Other than this, the selection of either the FW or the MS model for free energy seems to have little effect on the overall shape of transformation rate surfaces and the TCTT diagrams predicted from them.

The nucleation rate model includes several simplifying assumptions. Real isotropic−nematic phase transformation is unlikely to occur by nucleation of homogeneous spherical regions of order and also unlikely to grow uniformly in all directions. Thus, the homogeneous, spherical nucleus assumption used to calculate the rate (and later the TCTT diagrams) is inherently flawed. However, by simplifying the model, it provides a starting point for understanding the influence of the key variables in the system and demonstrates the feasibility of the kinetic calculations.

At the higher temperatures studied, nucleation is thermodynamically limited to high solution concentrations (this restriction is clearly seen in Figures 2 and 3). At lower temperatures, the composition region over which nucleation can occur is broader but the rates are reduced by diffusion limitations. The nucleation rate rises slowly from zero as the critical concentration is crossed and achieves a maximum at mesogen volume fraction equal to unity and well below T_{NI}—near 450 K for the FW method and 418 K for the MS method. The MS calculation predicts a less sudden rise in nucleation rate at high concentrations of mesogen and a larger region where the rate is a significant fraction of the maximum rate determined in our calculations, as shown by the contour plots in Figures 4 and 5. The unimodal results for rate are unsurprising given the opposite trends in mass transport and free energy of transformation with composition and temperature.

We reiterate that our approach here is necessarily a first-order one; limitations from the use of fixed β and Q values are obvious since both temperature and molar mass dependences can be expected for the former, with a molar mass dependence and possibly a solvent dependence for the latter. Furthermore, we assumed implicitly that the isotropic phase acts as a reservoir, and concentration and temperature do not change as the phase transformation progresses. Clearly, in a real system, the concentration in the isotropic phase will decrease with time and temperature gradients may arise. Nevertheless, results similar to those shown in Figures 4 and 5 are obtained for any combination of β and Q within the plausible range limits outlined above, suggesting that the trends in nucleation rate seen in the figures can be generally expected for isotropic-to-nematic phase transformation events. If either β or Q is set to an experimentally unrealistic value, the maximum nucleation rate moves to unrealistic conditions of low concentration or low temperature.

We plotted the Zeldovich factor (normalized by its maximum value) for the FW and MS energies (recall that z depends on absolute temperature, T, and $\Delta G_{a\text{-}i}$) in Figure 6 to illustrate its influence on the nucleation rate in each case. The Zeldovich factor scales as the square of transformation energy, and thus tends toward zero for small values of supersaturation or supercooling, and becomes large for extremely supersaturated and supercooled conditions. Consequently, the rate of nucleation is almost negligibly slow for supersaturation or supercooling conditions near the line of equilibrium with the isotropic phase (i.e., where $\Delta G_{a\text{-}i} = 0$). The net effect of the Zeldovich factor is that the peak in nucleation rate is shifted toward greater supersaturation and supercooling. When z is

DOI: 10.1021/cg501459m
Cryst. Growth Des. 2015, 15, 2620−2631

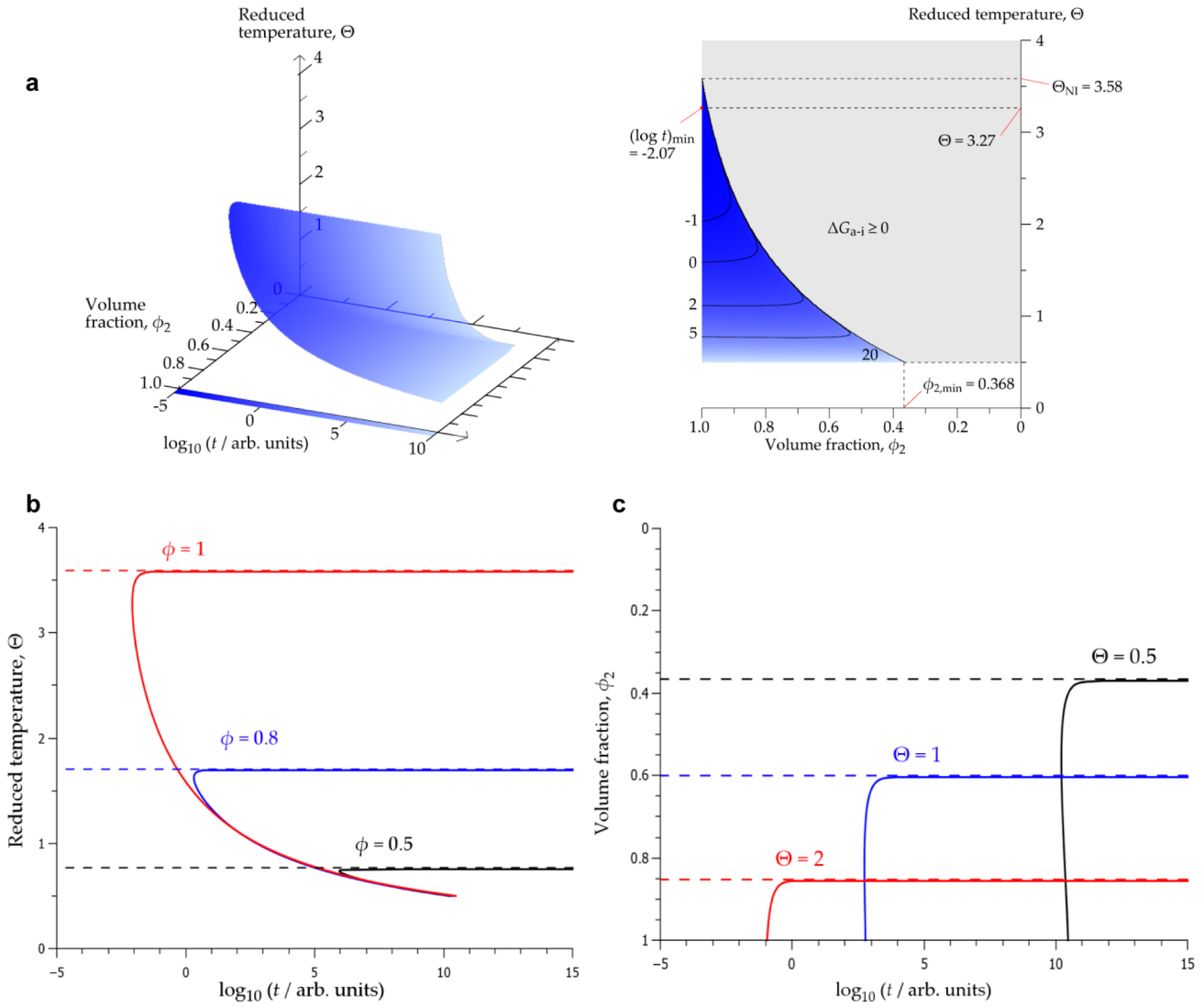

Figure 7. Contours of Y = 1% predicted from the FW free energy data of Figure 2 with Q = 2000 K, β = 3, and T^* = 167.6 K. The calculation result is presented as (a) TCTT diagram in isometric view and the view along the time axis, with black lines indicating contours of constant time, (b) TTT diagram at select concentrations indicated on the plot, and (c) TCT diagram at select values of reduced temperature. Note that the volume fraction axis is inverted in the TCT plot to match the axis orientation of the TCTT plot in a.

omitted from the rate calculation, there is a sharp rise in rate as the phase transition line is crossed, followed by a relatively slow decay in rate as the temperature is decreased and/or the concentration is increased. Including the z factor gives rise to the smooth "hill"-shaped rate curves seen in Figures 4 and 5.

TCTT Diagrams. We calculated the time required for Y = 1% of the isotropic solution to undergo phase transformation to the anisotropic (nematic) phase, shown in Figures 7 and 8 for the FW and MS approaches, respectively. The time scale in these plots does not consider certain proportionality constants (N_0, D_0) and is thus given in arbitrary units but is not otherwise normalized; the results are given using the non-normalized values for $\partial N/\partial t$ and z.

Example TTT and TCT plots are also shown for each case to clarify the behavior observed in the 3-D TCTT plots. The C-curve behavior is present in the TTT diagrams, with the time required to reach 1% decreasing rapidly over a very narrow region near the clearing temperature for a given volume fraction, reaching a minimum and slowly increasing as temperature is further lowered. In the TCT diagrams, the C curves appear cut off at the maximum value of unity for volume fraction. In both the FW and the MS approaches, the time to reach 1% appears more sensitive to temperature than to volume fraction of mesogen. The latter two effects may be due in part to divergence from the exponential relationship for the concentration dependence of mass transport at high volume fractions; the exponential form and corresponding decay constant used in this work come from literature data[53] for concentrations below about 0.12 volume fraction.

The utility of these plots—TTT, TCT, and TCTT—lies in recognizing the relatively small process windows that yield finite transformation times. Recall that the horizontal axis in all three plots is log-scale time. Thus, at least in some ranges of temperature and concentration, apparently small changes in the conditions of the phase transition are seen to precipitate orders-of-magnitude differences in processing time.

CONCLUSIONS

We have shown in our previous work[23,26] how the fundamental principles of nucleation and growth theory predict phase

DOI: 10.1021/cg501459m
Cryst. Growth Des. 2015, 15, 2620−2631

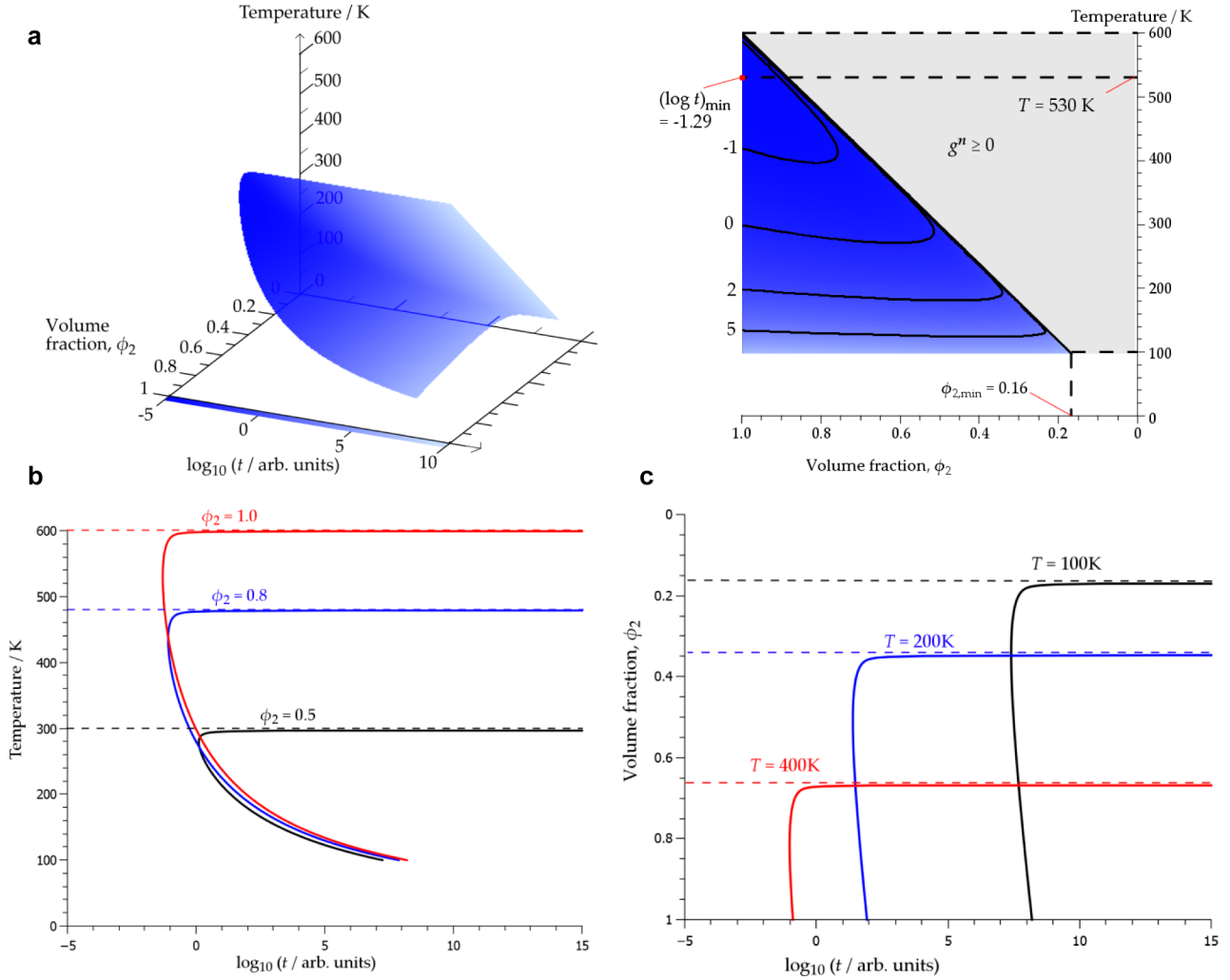

Figure 8. Contours of Y = 1% predicted from the FW free energy data of Figure 2 with Q = 2000 K, β = 3, and T_{NI} = 600 K. The calculation result is presented as (a) TCTT diagram in isometric view and the view along the time axis, with black lines indicating contours of constant time, (b) TTT diagram at select concentrations indicated on the plot, and (c) TCT diagram at select values of reduced temperature. Note that the volume fraction axis is inverted in the TCT plot to match the axis orientation of the TCTT plot in a.

transformation kinetics for a wide range of systems in which there is both a benefit of transitioning a reactant from one phase to another and a cost (e.g., energetic) of maintaining an interface between the two phases. Furthermore, we have shown how the predicted kinetic information can be presented graphically in a manner analogous to TTT diagrams. Here, we expanded on the approach laid forth by McEwen et al.[23] for semiquantitatively describing the concentration dependence of the rate of nematic phase formation, and we provided a specific application for our general model[26] by considering an isotropic-to-nematic phase transition simultaneously driven by composition and temperature changes. Calculation of the nematic−isotropic transformation energy is not new to this work but adds necessary detail to the model and enabled a first approximation of TCT and TCTT diagrams for this type of system.

The results of our calculations show reasonable trends for the nucleation energy, rate of stable nucleus formation, and TCTT curves as the degree of supersaturation and/or supercooling increases (i.e., as the conditions are moved further into the region where the isotropic to nematic transition is favorable). This work constitutes a successful first endeavor toward modeling concentration- and temperature-dependent phase transformation kinetics for the nematic ordering of idealized hard rod mesogens. Furthermore, the qualitative agreement of our results with the trends expected based on analogous temperature-driven phase transformations (e.g., the well-characterized eutectoid transformation in steels) bolsters the strength of the mathematical analogy of the two-variable model and also the general model.

Refinement of the model is needed to address the limitations and assumptions of the present work to permit accurate prediction of the TCTT diagrams for real systems. Such refinements include experimental efforts and/or additional calculation to obtain robust estimates for the parameters β, Q, D, N_0, and γ, accommodating any heterogeneous nucleation, nonspherical nuclei, and shape-dependent variations in nucleus surface energy. Consideration of the possibility of spinodal decomposition and more complex phase separation mechanisms[61,62] is also important to form a complete picture of possible phase transformations in some systems. Additional theoretical work is required to derive continuous transformation curves (i.e., for the scenario in which the

DOI: 10.1021/cg501459m
Cryst. Growth Des. 2015, 15, 2620−2631

composition and temperature are not quenched and held at constant values, as was assumed in this work).

We predict that accurate TCTT diagrams, obtained through higher order modeling and experiment, will provide convenient process design aids for promoting the formation of desired phases and avoiding undesired phase transitions in a variety of chemical systems. The present example of lyotropic liquid crystals is one of many possible applications; other example systems include control of polymorphic form during the production of active pharmaceutical ingredients (APIs), biopolymers, proteins, petroleum distillates, and food products. Finally, we reassert the notion[26] that the fundamental ideas behind TCTT diagrams may be of interest to researchers outside the domain of the physical sciences. The elegance of the general model lies in its ability to enable appropriate analogies to the ideas of the present work and to lead to similarly useful representations of temporal information for any system undergoing a transformation characterized by nucleation and growth.

■ ASSOCIATED CONTENT

Supporting Information

Detailed description of the mathematics used to compute the phase transformation energy for nematic ordering by the Maier−Saupe method; brief discussion of the effect of increasing the mesogen axial ratio in the Flory−Warner method. The Supporting Information is available free of charge on the ACS Publications website at DOI: 10.1021/cg501459m.

■ AUTHOR INFORMATION

Corresponding Author

*E-mail: cviney@ucmerced.edu.

Present Address

[‖]4 The Batch, Wincanton, Somerset BA9 9BN, United Kingdom.

Author Contributions

[‡]Jason Komadina and Stephen W. Watt contributed equally.

Notes

The authors declare no competing financial interest.

■ ACKNOWLEDGMENTS

J.K. and C.V. acknowledge support from UC Merced start-up funding. Useful insights regarding numerical methods were provided by Dr. Roderick Ferguson of Heriot-Watt University and are acknowledged here posthumously.

■ REFERENCES

(1) Volmer, M.; Weber, A. *Z. Phys. Chem., Stöchiom. Verwandtschaftsl.* **1926**, *119*, 277−301.
(2) Becker, R.; Döring, W. *Ann. Phys.* **1935**, *24*, 719−752.
(3) *Atlas of Isothermal Transformation and Cooling Diagrams*; American Society for Metals (ASM): Metals Park, OH, 1977.
(4) Doherty, R. D. Diffusive phase transformations in the solid state. In *Physical Metallurgy*, 3rd ed.; Cahn, R. W., Haasen, P., Eds.; North-Holland: Amsterdam, 1983; pp 933−1030.
(5) Honeycombe, R. W. K.; Bhadeshia, H. K. D. H. *Steels, Microstructure and Properties.*, 2nd ed.; Edward Arnold: London, 1995.
(6) Oxtoby, D. W. *Acc. Chem. Res.* **1998**, *31*, 91−97.
(7) Callister, W. D.; Rethwisch, D. G. *Fundamentals of Materials Science and Engineering*, 9th ed.; John Wiley & Sons, Inc.: New York, 2013.
(8) Shackelford, J. F. *Introduction to Materials Science for Engineers*, 8th ed.; Prentice Hall: New York, 2014.
(9) Davey, R. J.; Maginn, S. J.; Steventon, R. B.; Ellery, J. M.; Murrell, A. V.; Booth, J.; Godwin, A. D.; Rout, J. E. *Langmuir* **1994**, *10*, 1673−1675.
(10) Feher, G.; Kam, Z. Nucleation and growth of protein crystals: General principles and assays. In *Diffraction Methods for Biological Macromolecules Part A*; Wyckoff, H. W., Hirs, C. H. W., Timasheff, S. N., Eds.; Academic Press: Orlando, FL, 1985; Vol. *114*, pp 77−112.
(11) ten Wolde, P. R.; Frenkel, D. *Science* **1997**, *277*, 1975−1978.
(12) García-Ruiz, J.-M. *J. Struct. Biol.* **2003**, *142*, 22−31.
(13) Sear, R. P. *J. Phys., Condens. Mater.* **2007**, *19*, 033101.
(14) Auer, S.; Frenkel, D. *Adv. Polym. Sci.* **2005**, *173*, 149−208.
(15) Cuetos, A.; Dijkstra, M. *Phys. Rev. Lett.* **2007**, *98*, 095701.
(16) Wincure, B.; Rey, A. *Continuum Mech. Thermodyn.* **2007**, *19*, 37−58.
(17) Martínez-Felipe, A.; Badia, J. D.; Santonja-Blasco, L.; Imrie, C. T.; Ribes-Greus, A. *Eur. Polym. J.* **2013**, *49*, 1553−1563.
(18) Avramov, I. *Physica A* **2007**, *379*, 615−620.
(19) *Atlas of Time-Temperature Diagrams for Nonferrous Alloys*; ASM International: Materials Park, OH, 1991.
(20) *Aluminum and Aluminum Alloys*; ASM International: Materials Park, OH, 1993.
(21) Barsoum, M. W. *Fundamentals of Ceramics*; Institute of Physics Publishing: Bristol, U.K., 2003.
(22) Putnis, A. *Introduction to Mineral Sciences*; Cambridge University Press: Cambridge, U.K., 1992.
(23) McEwen, I. J.; Watt, S. W.; Viney, C. *Polymer* **2001**, *42*, 6759−6764.
(24) Viney, C.; Huber, A.; Verdugo, P. Processing biological polymers in the liquid crystalline state. In *Biodegradable Polymers and Packaging*, 1st ed.; Ching, C., Kaplan, D. L., Thomas, E. L., Eds.; Technomic: Lancaster, PA, 1993; pp 209−224.
(25) Viney, C.; Huber, A. E.; Dunaway, D. L.; Kerkam, K.; Case, S. T. Optical characterization of silk secretions and fibers. In *Silk Polymers: Materials Science and Biotechnology*, 1st ed.; Kaplan, D. L., Adams, W. W.; Farmer, B. L.; Viney, C., Eds.; American Chemical Society: Washington, DC, 1994; Vol. *544*, pp 120−136.
(26) Komadina, J.; Watt, S. W.; Viney, C. A Generalized Formalization of Nucleation and Growth for Traditional and Non-Traditional Contexts, and Its Application to the Concentration-Driven Crystallization of Proteins. Presented at the 2014 MRS Fall Meeting, Boston, MA, November 30−December 5, 2014, Paper NN6.10. http://www.prolibraries.com/mrs/?select=session&sessionID=5444 (accessed April 30, 2015).
(27) Ciferri, A.; Krigbaum, W. R. *Mol. Cryst. Liq. Cryst.* **1981**, *69*, 273−280.
(28) Pujolle-Robic, C.; Noirez, L. *Nature* **2001**, *409*, 167−171.
(29) Southern, J. H.; Porter, R. S. *J. Appl. Polym. Sci.* **1970**, *14*, 2305−2317.
(30) Odell, J. A.; Grubb, D. T.; Keller, A. *Polymer* **1978**, *19*, 617−626.
(31) Rey, A. D.; Herrera-Valencia, E. E. *Biopolymers* **2012**, *97*, 374−396.
(32) Flory, P. J. *Proc. R. Soc. London A* **1956**, *234*, 73−89.
(33) Flory, P. J.; Ronca, G. *Mol. Cryst. Liq. Cryst.* **1979**, *54*, 311−330.
(34) Warner, M.; Flory, P. J. *J. Chem. Phys.* **1980**, *73*, 6327−6332.
(35) Flory, P. J. *Adv. Polym. Sci.* **1984**, *59*, 1−36.
(36) Maier, W.; Saupe, A. *Z. Naturforsch.* **1959**, *14*, 882−889.
(37) Maier, W.; Saupe, A. *Z. Naturforsch.* **1960**, *15*, 287−292.
(38) Viney, C.; Yoon, D. Y.; Reck, B.; Ringsdorf, H. *Macromolecules* **1989**, *22*, 4088−4093.
(39) Flory, P. J.; Irvine, P. A. *J. Chem. Soc., Faraday Trans. 1* **1984**, *80*, 1807−1819.
(40) Shen, C.; Kyu, T. *J. Chem. Phys.* **1995**, *102*, 556−562.
(41) Chiu, H.-W.; Kyu, T. *J. Chem. Phys.* **1995**, *103*, 7471−7481.
(42) Brochard, F.; Jouffroy, J.; Levinson, P. *J. Phys. (Paris)* **1984**, *45*, 1125−1136.
(43) de Gennes, P. G.; Prost, J. *The Physics of Liquid Crystals*, 2nd ed.; Oxford University Press: New York, 1993.
(44) Twieg, R. J.; Chu, V.; Nguyen, C.; Dannels, C. M.; Viney, C. *Liq. Cryst.* **1996**, *20*, 287−292.

DOI: 10.1021/cg501459m
Cryst. Growth Des. 2015, 15, 2620−2631

(45) Watt, S. W. Factors that influence molecular packing in both liquid crystalline and related solid phases. Doctoral thesis, Heriot-Watt, Edinburgh, 2003.
(46) Mustafa, M. B.; Tipton, D. L.; Barkley, M. D.; Russo, P. S.; Blum, F. D. *Macromolecules* **1993**, *26*, 370−378.
(47) *Nucleation*; Marcel Dekker, Inc.: New York, 1969.
(48) Kelton, K. F. Crystal Nucleation in Liquids and Glasses. In *Advances in Research and Applications*, Ehrenreich, H., Turnbull, D., Eds.; Academic Press, Inc.: San Diego, CA, 1991; pp 75−177.
(49) ten Wolde, P. R.; RuizMontero, M. J.; Frenkel, D. *J. Chem. Phys.* **1996**, *104*, 9932−9947.
(50) Zeldovich, Y. B. *Zh. Eksp. Teor. Fiz.* **1942**, *12*, 525−538.
(51) Avrami, M. *J. Chem. Phys.* **1939**, *7*, 1103−1112.
(52) Avrami, M. *J. Chem. Phys.* **1940**, *8*, 212−224.
(53) Bu, Z.; Russo, P. S.; Tipton, D. L.; Negulescu, I. I. *Macromolecules* **1994**, *27*, 6871−6882.
(54) Krüger, G. J. *Phys. Rep.* **1982**, *82*, 229−269.
(55) Vilfan, M.; Lahajnar, G.; Zupančič, I.; Žumer, S.; Blinc, R.; Crawford, G. P.; Doane, J. W. *J. Chem. Phys.* **1995**, *103*, 8726−8733.
(56) Vilfan, M.; Vrbančič-Kopač, N.; Zalar, B.; Žumer, S.; Crawford, G. P. *Phys. Rev. E* **1999**, *59*, R4754−R4757.
(57) Williams, R. *Mol. Cryst. Liq. Cryst.* **1976**, *35*, 349−351.
(58) Faetti, S.; Palleschi, V. *J. Chem. Phys.* **1984**, *81*, 6254−6258.
(59) Doi, M.; Kuzuu, N. *J. Polym. Sci.* **1985**, *41*, 65−68.
(60) Chen, W. L.; Sato, T.; Teramoto, A. *Macromolecules* **1996**, *29*, 4283−4286.
(61) Soulé, E. R.; Rey, A. D. *Eur. Phys. J. B* **2011**, *83*, 357−367.
(62) Soulé, E. R.; Lavigne, C.; Reven, L.; Rey, A. D. *Phys. Rev. E* **2012**, *86*, 011605.

DOI: 10.1021/cg501459m
Cryst. Growth Des. 2015, 15, 2620−2631